
Feature-Based and Output-Based Grid Adaptation Study for Hypersonic Propulsive Deceleration Jet Flows

Hicham Alkandry¹, Michael A. Park², William L. Kleb³, and Iain D. Boyd⁴

¹ University of Michigan, halkandr@umich.edu

² NASA LaRC, Computational AeroSciences Branch, Mike.Park@NASA.gov

³ NASA LaRC, Aerothermodynamics Branch, Bill.Kleb@NASA.gov

⁴ University of Michigan, iainboyd@umich.edu

1 Introduction

The size requirements for conventional aerodynamic decelerators (parachutes) used to slow Mars entry vehicles during atmospheric descent are becoming unfeasible due to the increasing mass and landing site altitude of future missions. One alternative is propulsive decelerator (PD) jets. The use of PD jets, however, involves complex flow interactions that are still not well understood. Computational fluid dynamics (CFD) is currently being investigated as a tool for predicting these flow interactions. However, manually generating appropriate grids for these flows is difficult and time consuming because of the complexity of the flowfield. Therefore, automatic grid adaptation techniques present an attractive option to accurately capture the flow features and interactions. This study compares the grids and solutions for hypersonic PD jet flows using feature-based and output-based grid adaptation techniques.

2 Numerical Setup and Approach

The present study uses a scaled-down Mars Science Laboratory (MSL) aeroshell with a single-nozzle sonic PD jet located at the center of the forebody [1]. The 3-D computational domain consists of a quarter of the geometry due to symmetry. The freestream Mach number is 12, and the thrust coefficient of the PD nozzle, defined as the thrust force normalized by the product of the freestream dynamic pressure and the aeroshell frontal area, is 0.5. The freestream and the PD jet are modeled as perfect gas air in order to isolate the effects of mesh adaptation. The Reynolds numbers for the freestream (based on the diameter of the aeroshell) and the PD jet (based on the diameter of the nozzle-exit) are both roughly equal to 1,200, which suggests that both flows are laminar.

The numerical simulations are carried out using FUN3D (<http://fun3d.larc.nasa.gov>). FUN3D is a suite of codes developed at NASA Langley that includes a node-based 3-D Navier-Stokes equations solver for compressible flows. The solver uses the finite-volume method on unstructured grids to solve the set of partial differential equations. FUN3D also has feature-based and output-based grid adaptation capabilities that include parallel 3-D grid mechanics such as enrichment, coarsening, and element connectivity [3].

The feature-based adaptation in FUN3D targets local errors in the solution due to gradients of a specific flow variable [2]. For this study, the isotropic mesh density metric is given by the first derivative of the Mach number; and the anisotropic orientation and scaling metrics are computed by the second derivative tensor (i.e. Hessian) of the Mach number. The output-based (i.e. adjoint-based) grid adaptation method in FUN3D is a 3-D extension of the methods of Venditti and Darmofal [5] that adapts the mesh to reduce the simulation error in an output functional [4]. For this study, the output functional is chosen as the axial force on the vehicle, which corresponds to the drag force on both the aeroshell and the PD jet nozzle. The anisotropic metric is determined by a combination of the embedded-grid error estimation procedure and the Mach Hessian.

3 Results

Figure 1 shows the mesh and Mach number contours on the plane of symmetry for the initial, unadapted, grid. The mesh in Figure 1(a) includes an anisotropic region near the surface of the aeroshell to accurately capture the flow in the boundary layer. For the present study, this region is frozen and only the mesh outside this layer can be adapted automatically due to limitations in the current grid adaptation mechanics. The Mach number contours in Figure 1(b) illustrate the complex flow features that are generated due to the PD jet.

Table 1 provides the size of the initial and adapted grids. Limitations in the available computational resources cause the adaptation process to end after the 4th cycle. The feature-based method roughly doubles the number of nodes after each cycle and adds more points per cycle compared to the output-based method. The feature-based method inserts new nodes throughout the domain where local gradients are large. The output-based method only adds points where they improve calculation of the specified functional (axial force). The final feature-based adapted grid is over 3 times larger than the output-based adapted grid. The axial force coefficient (axial force normalized by the product of the freestream dynamic pressure and the aeroshell frontal area) is shown in Figure 2. This figure shows that the axial force coefficient for the feature-based and output-based adapted grids both converge to similar values as the number of nodes in the grid increases.

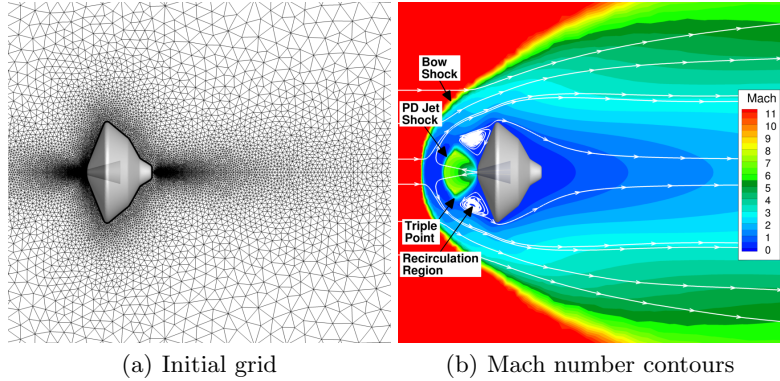


Fig. 1. Initial grid and solution (top half is reflected to bottom half).

Table 1. Grid size ($\times 10^6$ nodes).

	Feature-based	Output-based
Initial	0.7	0.7
1 st Cycle	1.6	1.5
2 nd Cycle	4.1	3.1
3 rd Cycle	10.2	4.3
4 th Cycle	23.7	7.7

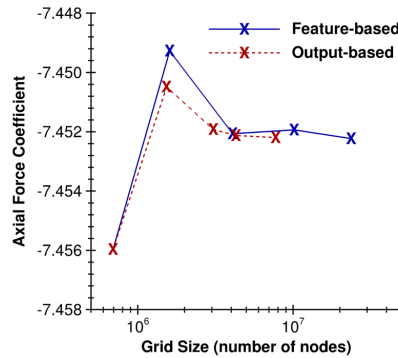


Fig. 2. Axial force coefficient.

Figure 3 shows the final adapted grids for the feature-based and output-based methods. The figure shows that the feature-based method adds more points than the output-based method near the downstream portion of the bow shock, at the boundaries of the recirculation zone and the PD jet, and in the expansion fans that develop around the shoulders of the aeroshell. The output-based technique inserts nodes on the stagnation streamline where freestream flow and PD jet mix. This stagnation region is ignored by the feature-based technique because of relatively weak gradients in this important region. The vertical stretching upstream of the bow shock in the feature-based adapted grid is currently being investigated.

Mach number contours on the plane of symmetry for the final adapted grids are shown in Figure 4(a), and a close-up view of the PD jet region is provided in Figure 4(b). The solutions for the two grids are in overall good agreement, except the downstream portion of the bow shock is thicker for the output-based adapted grid due to less grid resolution. The bow shock location

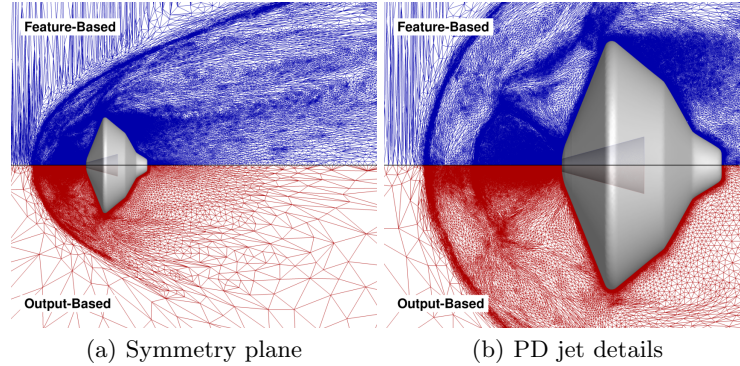


Fig. 3. Final adapted grids (top: feature-based; bottom: output-based).

along the stagnation streamline is also different for the two adapted grids by approximately 0.4%. Figure 4(c) compares the Mach number distribution at 0.15 aeroshell diameters away from the nozzle-exit (the dashed line in Figure 4(a)) for the initial and the final adapted grids. The figure shows overall good agreement between the solutions for the adapted meshes, but the initial grid produces thicker shocks due to coarse elements. A close-up view of the bow shock region at this axial location can be seen in Figure 4(d). The figure shows a difference of approximately 0.5% in the bow shock thickness between the solution for the adapted grids. These differences, however, have negligible effects on the axial force coefficient of the vehicle. For this particular case, the output-based method is roughly twice as fast as the feature-based method in terms of total computational time (i.e. time for all adaptation cycles).

4 Summary

This study compared the solutions and adapted meshes for a Mars entry aeroshell in Mach 12 flow with a single-nozzle sonic PD jet. The grids were adapted using feature-based and output-based methods for 3-D viscous flows. The study found that the feature-based adaptation technique roughly doubled the number of nodes in the grid after each adaptation cycle and overall added more nodes than the output-based technique. The feature-based method inserted more nodes near the downstream portion of the bow shock, at the boundaries of the recirculation zone and the PD jet, and in the expansion fans that develop around the shoulders of the aeroshell compared to the output-based method. The flowfield solutions for these two methods were in good agreement, but the thickness of the downstream portion of the bow shock was larger for the output-based since this region does not affect the value of the specified functional, the axial force on the vehicle. The axial force coefficients for the two methods were also in excellent agreement.

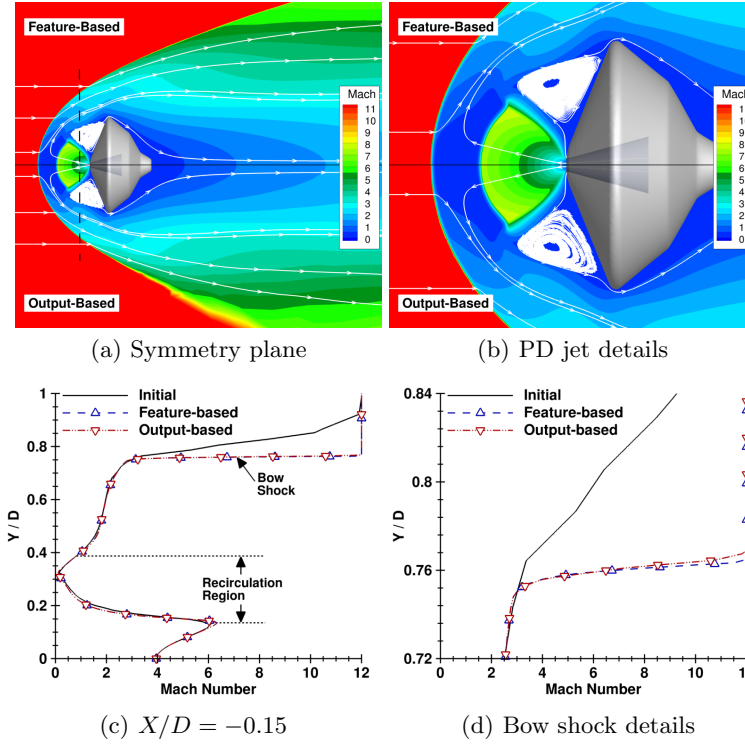


Fig. 4. Comparisons of Mach number contours (a, b) and distribution (c, d).

References

- [1] H. Alkandry, I. D. Boyd, E. M. Reed, J. R. Codoni, and J. C. McDaniel. Interactions of single-nozzle sonic propulsive deceleration jets on mars entry aeroshells. In *AIAA Paper 2010-4888*, June 2010.
- [2] K. L. Bibb, P. A. Gnoffo, M. A. Park, and W. T. Jones. Parallel, gradient-based anisotropic mesh adaptation for re-entry vehicle configurations. In *AIAA Paper 2006-3579*, June 2006.
- [3] M. A. Park. *Anisotropic output-based adaptation with tetrahedral cut cells for compressible flows*. PhD thesis, Massachusetts Institute of Technology, September 2008.
- [4] M. A. Park and J. R. Carlson. Turbulent output-based anisotropic adaptation. In *AIAA Paper 2010-0168*, January 2010.
- [5] D. A. Venditti and D. L. Darmofal. Anisotropic grid adaptation for functional outputs: application to two-dimensional viscous flows. *Journal of Computational Physics*, 187:22–46, 2003.